Soil Dynamics and Earthquake Engineering 131 (2020) 106034

Contents lists available at ScienceDirect

Soil Dynamics and Earthquake Engineering

journal homepage: http://www.elsevier.com/locate/soildyn

Liquefaction resistance of Fraser River sand improved by a microbially-induced cementation

Guillermo Alexander Riveros, Abouzar Sadrekarimi *

Department of Civil and Environmental Engineering, Western University, London, Ontario, Canada

ARTICLE INFO

Keywords:
Cyclic simple shear test
Liquefaction resistance
Microbial-induced calcite precipitation
Shear wave velocity

ABSTRACT

Microbially induced calcite precipitation (MICP) harnesses the natural metabolic action of bacteria to induce the precipitation of calcium carbonate and alter soil engineering properties. This paper presents the results of using MICP to improve the cyclic resistance of Fraser River sand specimens. The formation of calcite cementation among sand particles is confirmed using scanning electron microscopic images and X-ray compositional analysis of cemented sand clusters. The results show that the velocity of a shear wave (V_S) traveling through the specimen starts to increase just as the calcium solution is introduced into each specimen. Liquefaction resistance of sand samples is subsequently measured in a series of cyclic direct simple shear tests. MICP-treated samples exhibit cyclic resistances of up to 67% higher than those of the untreated sand. Post-liquefaction volumetric strain and changes in cyclic resistance in a repeated cyclic loading are also assessed and compared for the original and the treated sand specimens.

1. Introduction

Despite being the least abundant element in the Earth's crust [1], carbon is commonly found on the planet's surface as large reservoirs of organic matter or as inorganic carbon in carbonate rocks such as limestone [2]. Many organisms mediate in what is known as the "carbon cycle", by fixing inorganic carbon to form organic carbon and re-mineralizing organic carbon back to inorganic carbon. Particularly, bacteria facilitate the deposition of carbonate minerals on the Earth's surface by precipitating calcium carbonate ($CaCO_3$) extracellularly as a result of their metabolic process [3–5]. In an environment with a sufficient concentration of calcium ions (Ca^{2+}), $CaCO_3$ precipitation can be stimulated by a microbial metabolism that increases the pH and the concentration of carbonate ions (CO_3^{2-}) on the cells' surface. These cells in turn serve as nucleation sites for the precipitated mineral. This process is generally referred to as a "microbially induced calcite precipitation (MICP)" and can occur via different metabolic processes.

MICP via urea hydrolysis involves the use of the microbial enzyme urease (urea amidohydrolase; EC 3.5.1.5) to hydrolyze or break down the organic compound urea. Urease positive bacteria, such as Sporosarcina pasteurii, use urea as a source of nitrogen and energy [6] and produce the enzyme urease at different levels depending on the bacterial strain [7]. Precipitation of $CaCO_3$ typically begins with the formation of an amorphous form of $CaCO_3$ with low stability and high solubility, followed by a transformation into a metastable and transitional phase known as vaterite, and ending in the subsequent transformation into a more thermodynamically stable state as calcite [8]. In a soil, the precipitated calcium carbonate can cement soil particles and fill void spaces. An alkaline environment with pH = 8.3 to 9.5 [6,9] is critical to trigger the hydrolysis of urea. If the pH level becomes acidic (<7.0), the precipitated $CaCO_3$ will begin to dissolve as opposed to fostering further precipitation in the above chain of reactions. A local rise in pH may also cause the microbes themselves to serve as nucleation sites for calcite formation on the surface of bacterial cells [10].

The biological nature of MICP has made it an appealing and environmentally-friendly process to improve the cyclic resistance and liquefaction behavior of sandy soils [11–15]. In dynamic centrifuge model tests on a thick deposit of loose Ottawa 50/70 sand, Montoya et al. [12] demonstrated that MICP treatment increased liquefaction resistance and reduced excess pore pressure following the application of a cyclic load. Han et al. [13] found that microbial cementation improved the cyclic liquefaction resistance of a poorly-graded sand by as much as that achieved by chemical silica grouting, but within a much shorter time period. In cyclic triaxial tests on three different types of silica sands, Zamani et al. [15] observed that the improvement in cyclic resistance due to MICP treatement was dependent on the size and the shape of sand

* Corresponding author.
E-mail addresses: griveros@uwo.ca (G.A. Riveros), asadrek@uwo.ca (A. Sadrekarimi).

https://doi.org/10.1016/j.soildyn.2020.106034
Received 31 July 2019; Received in revised form 29 December 2019; Accepted 2 January 2020
Available online 16 January 2020

particles. Sands with more angular particle shapes or with smaller particle sizes achieved higher levels of improvement. Indigenous bacteria in natural soil have also been stimulated to induce $CaCO_3$ precipitation. Burbank et al. [11] treated a natural alluvial sand with an enriched solution of molasses and urea to promote the growth of native bacteria which use urea as a nitrogen source. Their laboratory cone penetration tests indicated a large increase in tip resistance after treatment relative to the untreated sand. Cyclic triaxial testing also showed a remarkable increase in cyclic resistance by 2.5 to 4.5 times that of the untreated samples. The significant improvement in cyclic resistance was attributed to the highly uniform precipitation of $CaCO_3$.

Several factors control the feasibility and the effectiveness of an MICP treatment in a soil. These include bacterial activity, pore throat size, pH level, composition of the treatment recipe, frequency of treatment, as well as the mineralogical composition of a soil [16]. Pore throat sizes in a soil matrix control the ease of microbial flow and therefore the distribution of bio-cementation in a soil [17–19]. Using the particle diameter larger than those of the 10% of a soil's mass (D_{10}) to represent a soil's mean pore throat size, Mitchell and Santamarina [17] present Fig. 1 as an approximate guideline to identify the range of soil pore sizes which can be treated by common bacteria. The region between boundary lines 1:2 and 1:200 in this figure represent the range of D_{10} suitable for biological activity.

As shown in Fig. 1, the effect of bacterial mineral precipitation depends on the size of pore spaces, besides several other factors. This study examines the effect of a biological treatment on the cyclic shearing behavior and liquefaction resistance of Fraser River sand using bender element and direct simple shear tests. Fraser River sand is an alluvial deposit found in the Fraser River Delta. Located in the lower mainland of British Columbia, Canada, this area (including Metro Vancouver) is one of the most populated and fastest growing regions in Western Canada. However, because of its location between major tectonic plate boundaries, there is a high risk of a large earthquake and liquefaction failure of thick deposits of loose Fraser River sand underlying this area [20,21]. A widespread liquefaction and lateral spreading could damage major bridges, roads, and utilities, and disrupt operations of the Vancouver International Airport, the Tsawwassen Ferry Terminal, the Roberts Bank Deltaport, as well as the major submarine transmission cables and pipelines [22]. This is the first experimental study aimed at demonstrating the application of an MICP treatment to improve the cyclic liquefaction resistance of Fraser River sand. With the objective of better understanding the treatment's effects, only a single application of the treatment is studied.

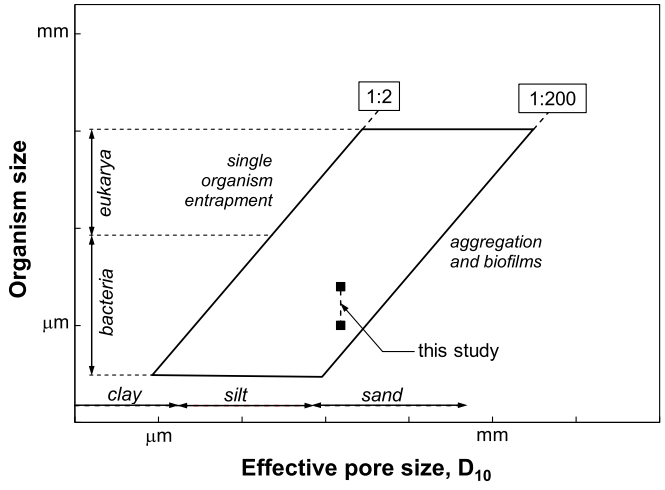

Fig. 1. Microorganism size limits for treatment of soils (after Mitchell and Santamarina [17]).

2. Description of materials used

2.1. Microorganism and growth conditions

Sporosarcina ureae (referred to as *S. ureae* hereafter) was used in this study for the treatment of Fraser River Sand through MICP. *S. ureae* is an endospore-forming, urease-positive, motile, aerobic bacterium, with optimum growth temperature and pH of 25 °C and 7, respectively [23]. This species is commonly found in soil and can tolerate pH levels of up to 10. Cells are round to oval with a diameter of approximately 1.0–2.5 µm and may grow individually, in pairs, tetrapads, or in packets of eight or more cells by division in two or three perpendicular planes. As shown in Fig. 2, colonies are creamy in colour, turning yellowish in a nutrient agar medium. Same as all bacterial cells, *S. ureae* possesses small bristle-like external fimbriae which facilitate the clinging of cells as solid microbial colonies in Fig. 2a, or as a liquid biofilm in Fig. 2b [24]. As a crucial requirement in MICP treatment, the urease in *S. ureae* has been found to be remarkably active with an enzymatic activity of greater than 9300 µmol urea hydrolyzed per minute for each milligram of protein at a pH of 7.5 [25].

For the preparation of growth medium and chemical reagents, all equipment and individual solutions were first sterilized to prevent contamination with unwanted foreign species. Given that *S. ureae* has been observed to grow well on peptone-containing media [26], nutrient agar and broth containing 22% peptone and 13% beef extract were used as solid and liquid growth media, respectively. Colonies were first plated on petri-dishes (5.5 cm dia.) with nutrient agar (23 gr/L) as the source of energy and incubated for a period of 24 h at a temperature of 25 °C. A

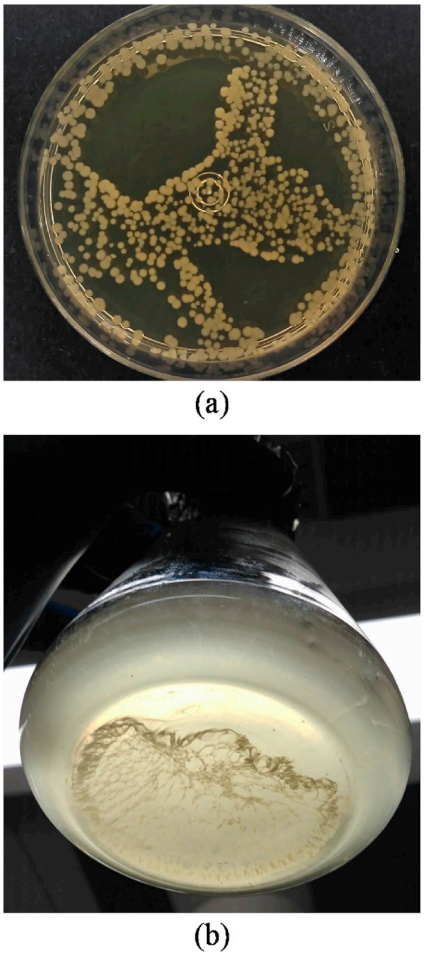

Fig. 2. Sporosarcina ureae cultured as (a) solid colonies, and (b) a liquid biofilm media.

single colony was subsequently inoculated in 30 mL of a nutrient broth (8 gr/L) with a pH = 7.17 and incubated aerobically at 25 °C without agitation.

Bacterial growth was continuously monitored by means of a UV–Vis spectrophotometer (HACH DR6000). An absorbance spectrophotometer is an instrument that measures the amount of light a solution absorbs by comparing the intensity of incident light reaching the sample with the intensity of light passing through it. Because suspended particles in a given compound cause the scattering of light, a spectrophotometer is used to estimate the number of bacterial cells in suspension for microbiological applications. A higher bacterial concentration in a liquid culture results in a higher absorbance of light. In this case, absorbance is referred to as Optical Density (OD_ξ), where ξ is the wavelength of light used in a spectrophotometer test. Because organic materials exhibit a higher optical density under light with ξ = 600 ηm, readings are commonly taken as OD_{600}. Measurements in a sample relative to a blank reference liquid containing everything in the sample except the cells being analyzed (i.e. plain media vs. inoculated media) provides an estimate of the bacterial cell concentration in the liquid, which can be subsequently used to estimate the growth phase of the population cell.

In order to determine the amount of time required to reach a stationary growth phase for *S. ureae* and measure the maximum cell density, series of 1.0 mL resuspended cultures were placed in 1.5 mL polystyrene cuvettes and tested in the spectrophotometer at various time intervals. Since only the optical density of the multiplying suspended particles was of interest, a sample of the pure nutrient broth was used as a blank. By measuring OD_{600} at different time intervals, the stationary growth phase of *S. ureae* was reached approximately 7 days (10,000 min) after inoculation, as shown in Fig. 3, with $OD_{600} = 1.2$ by the two distinct trials. Accordingly, the incubation of bacteria was stopped after 7 days by storing the harvested bacteria in a refrigerator at 4 °C to minimize their activity and the formation of dead bacterial cells.

A statistical procedure was followed in this study to estimate the number of viable bacterial cells by serial dilution. In this method, four (4) series of ten-fold dilutions were carried out by successively mixing 1 mL of bacterial liquid culture in 9 mL of autoclaved-sterilized water (i.e., volumetric ratio of 1:10) to reduce the number of bacterial cells to a countable concentration (300–30 colonies). From each of the dilutions, 10% of volume (1 mL) was taken and plated on an agar petri dish. The colony forming units (CFUs) on the petri dish were counted in each series and multiplied by the total dilution factor of that series. Ultimately, 50 colonies were counted on a petri dish plated after the fourth dilution (10^4), resulting in 5×10^5 CFU per 1.0 mL volume of the liquid culture. This cell density falls within the ranges of CFU and viable cell counts used by other researchers investigating the effectiveness of MICP [27–30].

2.2. Preparation and optimization of reagents

The biochemical reactions involved in urea hydrolysis increase the local pH of the solution due to the generation of hydroxide ions (OH^-) and ammonium ($NH4^+$). Accordingly, pH measurements can be used to monitor the progress of urease activity [6,31]. Fig. 4 presents the observed changes in pH with time, measured using a digital pH meter (Mettler Toledo) after mixing 15 mL of *S. ureae* stock (inoculum size: 5×10^5 CFU/mL) with 15 mL of urea at two different concentrations. The two mixtures were maintained at a room temperature of 22 °C. As shown in Fig. 4, the initial pH of the harvested stock was 8.4. However, for both trials a limiting pH value of approximately 9.2 was reached after 48 h as the concentration of products resulting from the hydrolysis of urea increased. This suggests that the concentration of urea was not a limiting factor in the enzymatic activity. Instead, the continuously increasing pH caused the rate of urea hydrolysis to decrease, reaching a stagnant point at pH > 9. Similar observations have also been reported by several other investigators [6,32,33] using other types of ureolytic bacteria.

Given that ureolysis reactions are largely controlled by the microorganism type, the mole ratios of different constituents cannot be used to estimate reagent concentrations required to yield a predetermined concentration of precipitated $CaCO_3$ (e.g., 1 mol of urea will not result in 1 mol $CaCO_3$). Therefore, an experimental optimization program shown in Fig. 5 was developed to establish treatment reagent concentrations which would enhance the precipitation of $CaCO_3$. In this figure, pH_i and pH_f are respectively the initial and the final pH before and after adding specific compounds. A standard urea solution was prepared and filter-sterilized at a concentration of 0.5 M (or 3% by volume) to enhance the growth of *S.ureae* [23]. Note that urea was not added to the growth medium at this stage, as the combined processes of population growth and urea hydrolysis would have occurred simultaneously, altering the OD_{600} meant to serve only as an index of growth. As part of the optimization program, three separate laboratory tests were conducted in similar autoclaved Erlenmeyer flasks containing 30 mL samples of *S. ureae* stock mixed with 30 mL of 0.5 M urea solution and maintained at room temperature. At the room temperature, the previously refrigerated bacteria were reactivated in the urea solution. The pH_i measured after the first hydrolysis cycle (48 h) averaged 9.3 for all three tests. In the first stage, Test 1 was driven to induce $CaCO_3$ precipitation by mixing in 30 mL of autoclaved 0.75 M $CaCl_2$. In Tests 2 and 3, the pH_f of stock mixtures was reduced by adding 5 mL of autoclaved 0.8 M (or 5% by volume) acetic acid to each solution, in order to reactivate enzymatic activity and begin a new hydrolysis cycle. As a result of urea hydrolysis,

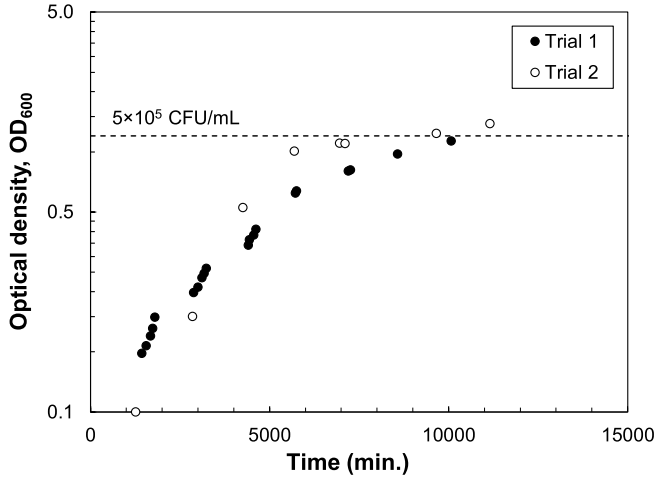

Fig. 3. Growth curve for Sporosarcina ureae in a liquid broth medium.

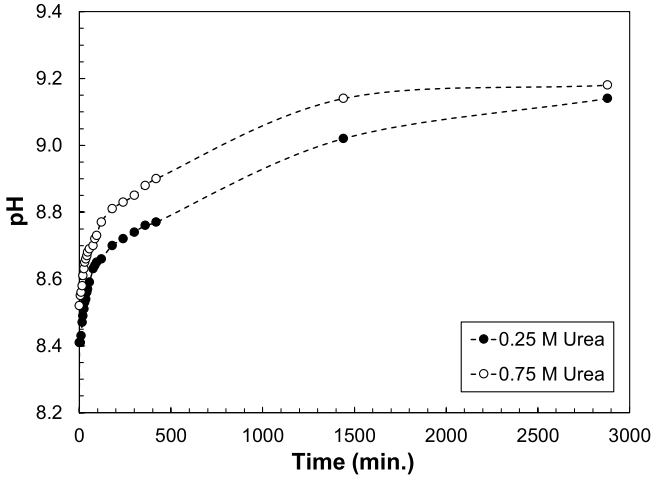

Fig. 4. Changes in pH during urea hydrolysis for two different concentrations of urea.

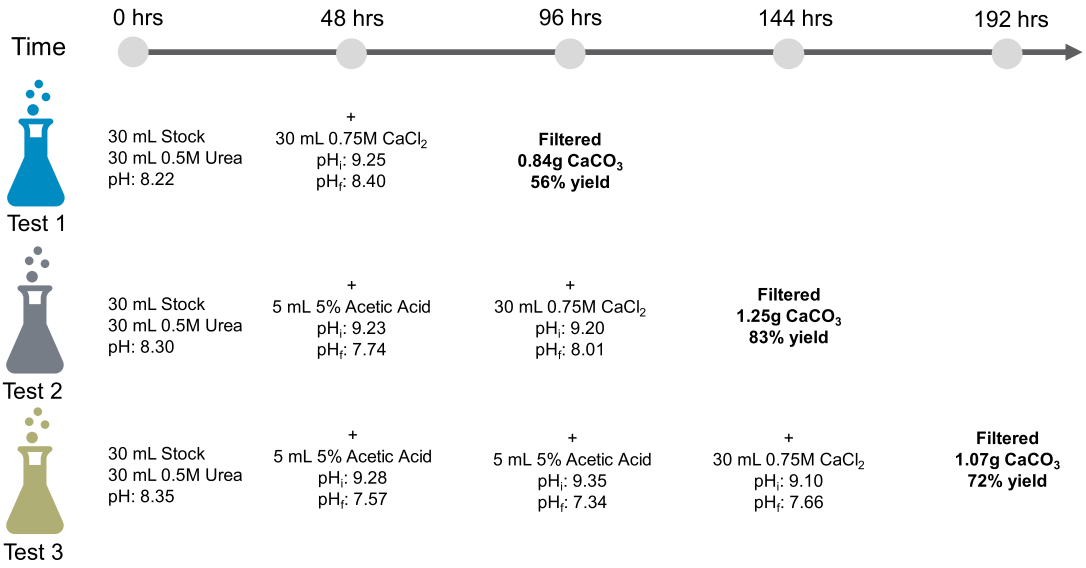

Fig. 5. Laboratory optimization program for biomineralization of $CaCO_3$. pH_i and pH_f are respectively the initial and the final pH before and after adding specific compounds.

a higher pH_i was reached in each cycle. $CaCl_2$ was chosen as the calcium source as it would precipitate the most stable form of $CaCO_3$ [33–35]. Two days later, the amount of $CaCO_3$ precipitate in Test 1 was filtered from solution, air-dried, and compared with the theoretical chemical yield, resulting in 56% yield. In the second stage, Test 2 was driven to induce $CaCO_3$ precipitation by mixing in 30 mL of autoclaved 0.75 M $CaCl_2$, while pH_f of the stock mixture for Test 3 was reduced a second time by adding another 5 mL of 5% acetic acid. After an additional 48 h period, the amount of $CaCO_3$ precipitated in Test 2 was weighed and compared with the theoretical chemical yield, resulting in 83% yield. Finally, Test 3 was driven to induce $CaCO_3$ precipitation by mixing in 30 mL of autoclaved 0.75 M $CaCl_2$. As with the previous tests, the amount of $CaCO_3$ precipitated in Test 3 was weighed and compared with the theoretical chemical yield, resulting in 72% yield.

Based on the observed results, the reagent concentrations used in Test 2 and summarized in Table 1 were selected as the basis for the biocementation treatment applied to the sand specimens in this study. The biological solution contained the cultured stock along with the compounds produced after two cycles (96 h) of urea hydrolysis. The cementation reagent contained calcium chloride, supplemented with 2/3 by volume of dissolved urea in order to foster further $CaCO_3$ precipitation after injecting the reagent.

The mineralogy of the $CaCO_3$ precipitate was subsequently examined using a powder X-ray diffractometer (Rigaku RINT 2500) with Cu–K radiation ($\xi = 1.54$ Å). Fig. 6 presents the diffraction pattern as a series of reflections with varying intensities at different values of twice the X-ray striking angle, 2θ [36]. Each mineral crystal is identified through the unique and distinct three-dimensional spacings among its interatomic planes using the reflected X-ray's wavelength and the Bragg's law. According to Fig. 6, the mineral phases identified in the precipitate are calcite (74%) and vaterite (26%), which are the most common phases of $CaCO_3$ polymorphs produced by MICP [37,38]. Note that vaterite is a less stable form of $CaCO_3$ [39], often formed in the presence of colloidal silica, iron pyrites [40], or organic compounds such as those produced by microbial activity [38,41]. The amounts of each phase (i.e., % by weight) were estimated from a reference intensity ratio anlaysis of the diffraction pattern, which involved the comparison of intensity peaks with predetermined standard values from reference databases [42,43].

Table 1
MICP treatment reagents employed in this study.

Reagent	Contents
Biological solution	15 mL bacterial stock (5×10^5 CFU/mL of *S. ureae*) + 15 mL 0.5 M urea +5 mL 0.8 M acetic acid
Cementation reagent	30 mL 0.75 M $CaCl_2$ + 20 mL urea

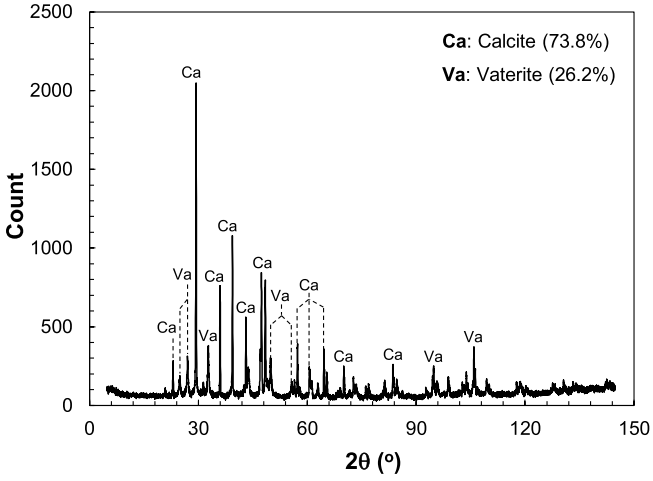

Fig. 6. X-ray diffraction compositional analysis of the $CaCO_3$ precipitate.

2.3. Description of material tested

Fraser River sand samples were obtained from an excavation site in Richmond, British Columbia near the north arm of Fraser River. Fig. 7 shows a scanning electron microscopic (SEM) image of the sand particles, displaying their generally sub-angular to angular shapes. X-Ray diffraction analysis describe the sand's mineralogical composition as 55% orthoclase feldspar, 35% quartz, and 10% muscovite [44].

Sieve analysis were conducted to determine the particle size distribution of Fraser River sand in compliance with ASTM D-422 standard procedure [45]. The average gradation is shown in Fig. 8, which classifies the material as a poorly graded clean sand (SP) per the Unified Soil Classification System (USCS). Other index characteristics including the

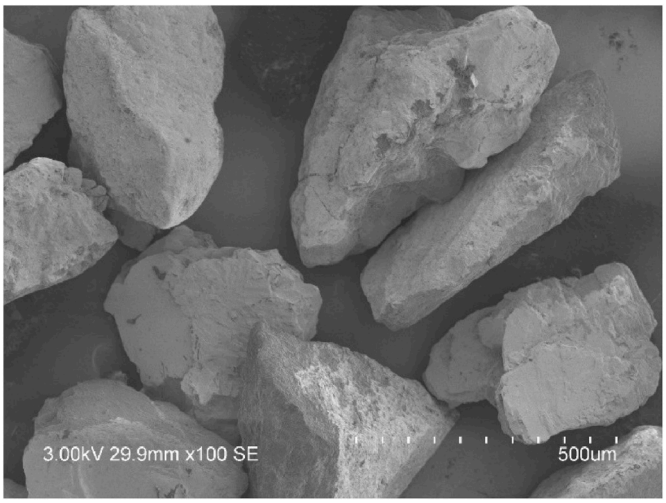

Fig. 7. SEM image of Fraser River Sand particles showing angular to sub-angular shape.

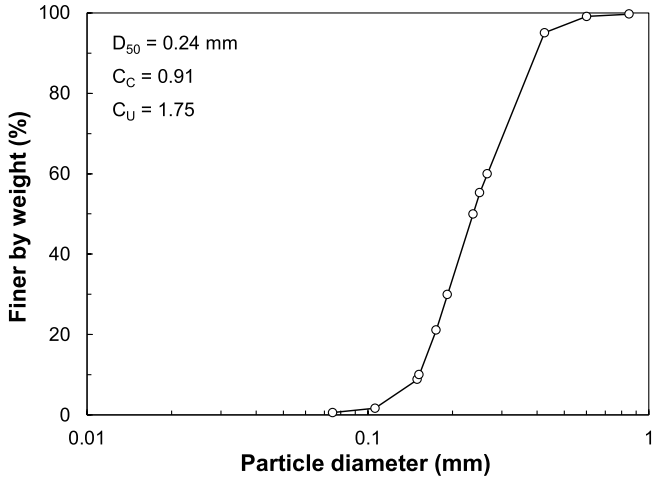

Fig. 8. Particle size distribution of the Fraser River sand used in this study.

maximum (e_{max}) and minimum (e_{min}) void ratios, and the specific gravity of sand particles (G_S) of respectively 0.96, 0.63, and 2.69 were also determined following ASTM standard methods [46–48]. Furthermore, with a D_{10} = 0.15 mm, the organism-to-particle size ratio of *S. ureae* and Fraser River sand ranges from 1:60 to 1:150, falling within the bounded region in Fig. 1 for the suitability of microbiological treatment.

3. Experimental method

3.1. Equipment used

Laboratory shear tests were conducted at the University of Western Ontario using an advanced cyclic direct simple shear (DSS) testing device (manufactured by GDS Instruments) equipped with bender elements for the measurement of shear-wave velocity (V_S). The DSS device includes a vertical electro-mechanical actuator for applying vertical stress, and a horizontal actuator that allows the application of simple shearing to a soil specimen. The vertical actuator has a displacement range of 50 mm and a maximum force capacity of 5 kN. The horizontal actuator has a displacement range of 25 mm with a maximum load capacity of 2 kN. When mounted, a specimen is axially confined between the upper and the lower pedestals of the DSS mold. A stack of Teflon-coated stainless-steel rings provide a rigid radial boundary for the specimen while allowing unrestricted application of horizontal displacement during shear. Specimen saturation is accomplished by flushing water through the inlet and outlet connections in the top and bottom pedestals, allowing the ingress of water through sintered porous disks into the specimen. A latex membrane, secured by O-rings at the top and bottom pedestals, prevents the leakage of pore water.

The bender elements inserted into the DSS pedestals consist of small cantilever piezoelectric plates which are shallowly embedded at the top and bottom of the specimen during confinement. A voltage signal is transmitted to one of the bender elements, which subsequently converts this signal to a sinusoidal mechanical vibration with a set wavelength by means of its piezoelectric properties. The shear wave propagating through the sample is then received by the other bender element and converted back to an electric voltage signal.

3.2. Sample preparation

Several studies have obtained relatively uniform void ratios in samples prepared by moist tamping [49–51]. To prepare loose samples with reasonably uniform void ratios which would undergo liquefaction during undrained shearing, specimens for both the untreated and treated experiments of this study were prepared by moist tamping. Specimen preparation procedures are briefly described in the following paragraphs.

3.2.1. Untreated samples

Untreated specimens were prepared by mixing dry sand with 5% by weight of distilled water. The moist sand was subsequently scooped and tamped to the desired specimen height inside the DSS device's mold. Moisture in the sand structure creates a capillary effect among sand particles, producing a very loose fabric that can be readily molded. The void ratio of each specimen was controlled by varying the weight of dry sand tamped into the specimen mold. The sample mold consisted of a bottom steel pedestal which supported a stack of Teflon-coated steel rings internally lined with a latex membrane (0.82 mm thick). The steel rings had an inner diameter of about 71.96 mm and a thickness of 1.05 mm each. Given the constraints in size provided by the rings' inner diameter and the latex membrane, all specimens were prepared with a diameter of 70.3 mm.

3.2.2. Samples for MICP treatment

Sand specimens for biological treatment were prepared in a similar manner to those for untreated testing. For these specimens, however, the dry sand was first sterilized in an autoclave and then mixed with 10% by weight of the biological solution to create a more uniform distribution and retention of bacteria on particle surfaces. The bacterial solution was pre-mixed with dry sand instead of being flushed through the sand after sample preparation, as the finely porous disks in the upper and lower pedestals (which ultimately confined the specimen) would act as filters, thus impeding a high concentration of cells from reaching the sand. An hour of retention time was allowed for the bacteria to attach on the surfaces of the sand particles.

3.3. DSS and bender element tests

3.3.1. Consolidation and saturation

Untreated specimens tested in the DSS device were initially loaded to a vertical seating stress of 5 kPa and saturated with de-aired water by means of a differential pressure head system at a rate of approximately 0.83 mL/min. These samples were subsequently consolidated to the target vertical stress (σ'_{vc}) until the rate of vertical deformation significantly reduced, thus indicating the end of primary consolidation. Conversely, the MICP-treated specimens were first consolidated to the target σ'_{vc} prior to injecting the cementation reagent to preserve the integrity of the cementation bonds. Once the vertical deformation

appeared to have stabilized (reaching the end of primary consolidation), the samples were slowly flushed with approximately 40 mL of the cementation solution by means of a differential pressure head system at a rate of approximately 0.83 mL/min. Samples were left to cure for 7 hours at a room temperature of 22 °C while maintaining a constant σ'_{vc}. Finally, deaired and deionized water was flushed through the specimens to remove the effect of matric suction in the moist-tamped specimens as well as the residual $CaCl_2$ and other chemicals. Full saturation was reached once air bubbles were no longer visible leaving the drainage tube, and the specimen volume change was re-stabilized. Note that carbon dioxide flushing, as commonly used for saturating sand specimens, was not applied to avoid acid generation and the degradation of calcite cementation.

3.3.2. Bender element tests

The amount of precipitated calcite is often not a valid indicator of MICP-induced improvements of soil mechanical characteristics [52–54]. This is due to variations in soil fabric and uniformity of calcite distribution produced by the precipitation environment (e.g. temperature, urease activity). Accordingly, instead of calcite content, V_S was used here to capture the increase in small-strain stiffness of the sand matrix as an indirect measurement to monitor biochemical activity and cementation level at particle contacts in real time. Baseline bender element tests were first performed on untreated specimens to determine V_S of the original Fraser River sand. In these specimens, V_S was measured soon after the consolidation stage when changes in vertical displacement had stabilized. For the MICP-treated samples, V_S measurements were taken after injecting the cementation reagent and monitored until V_S was observed to stabilize. Several methods for interpreting a shear wave signal have been proposed [55,56], with the peak-to-peak method proven to provide accurate measurements of V_S [57,58]. In this method, which was also used in this study, the travel time (Δt) is defined as the time difference between the peaks of the incipient wave and the first received wave. The shear wave travel distance is taken as the tip-to-tip distance between the bender elements along the specimen height [57]. Near-field effects caused by compression waves and electrical noise [55, 59–61] were also minimized by generating shear waves at an excitation frequency of 33.3 kHz to produce a shear wavelength of less than half of the specimen height.

3.3.3. Cyclic simple shear tests

Cyclic DSS tests were carried out on specimens consolidated to average relative densities (D_{rc}) of 65, 52, and 22% at σ'_{vc} = 100 kPa. Cyclic shearing was carried out while maintaining a constant-volume condition in order to observe the undrained shearing behaviour of the sand specimens. In these tests, no shear-induced pore water pressure was produced and the changes in total vertical stress required to maintain a constant specimen height were taken as the equivalent pore water pressure which would have been produced in a truly undrained test on a saturated sample [62–66]. As pore water pressure was not measured, the drainage tubes attached to the sample were left open to allow complete drainage of excess pore pressure in the sand samples. Cyclic shear loading is specified in terms of a cyclic stress ratio (CSR), defined as the ratio of the applied shear stress (τ_{cyc}) to σ'_{vc} as below:

$$CSR = \frac{\tau_{cyc}}{\sigma'_{vc}} \quad \text{(Eq. 1)}$$

Shear strain is also calculated as the horizontal displacement of the specimen's top platen divided by the specimen's height prior to shearing. Like many other researchers [65,67,68], cyclic shearing was applied at a frequency of 0.1 Hz in order to obtain consistent and stable cyclic stress paths. MICP-treated specimens consolidated to D_{rc} = 52% and 65% were subjected to an additional cyclic shearing stage after the first liquefaction event by zeroing the shear load, reconsolidating the specimen to the same σ'_{vc} = 100 kPa, and subsequently re-applying the same CSR as in the first cyclic shearing stage. This was done in order to compare the specimens' cyclic shearing behaviour and re-liquefaction resistance with that exhibited in its first liquefaction event. As previously described, two series of bender element and direct simple shear tests were conducted, namely those performed on untreated specimens and those done on MICP-treated samples. In summary, the testing program comprised 25 cyclic DSS tests as well as 25 measurements of V_S using bender elements.

4. Test results

4.1. Shear wave velocity

V_S was recorded in the treated samples approximately 48 hours after the application of treatment when V_S had stabilized and reached a constant value. For example, Fig. 9 shows a sharp increase in V_S of about 50 m/s at the onset of injecting the cementation reagent which is produced by the initial bonding of microbes on particle surfaces. V_S continues to increase with time, ultimately gaining about 90 m/s and reaching a maximum limit of 275 m/s in 48 hours after which no further increase is observed. This is similar to V_S increments of 110 and 94 to 98 m/s, observed by respectively Montoya and DeJong [53] and Safavizadeh et al. [69] in microbial cementation treatments of Ottawa 50/70 sand and fly ash specimens. The rise of pH in the treated sample is also superimposed on Fig. 9. The similar rates of increase in pH and V_S indicates that the precipitation of $CaCO_3$ was the result of an increase in the concentration of urea hydrolysis products with time.

V_S is often normalized with respect to the effective overburden stress in order to account for the effect of σ'_{vc} as below [70]:

$$V_{S1} = V_S \left(\frac{P_a}{\sigma'_{vc}}\right)^{\beta} \quad \text{(Eq. 2)}$$

where, V_{S1} is the overburden stress-normalized shear wave velocity, β is the stress normalization exponent, and P_a is a reference pressure (= 100 kPa). Fig. 10 shows that V_S measured in the untreated samples (with D_{rc} = 16–36%) increases from about 149 m/s to a maximum of 303 m/s with the increasing of σ'_{vc} from 50 to 900 kPa. These data show a general trend which is fitted with a power function using β = 0.25, irrespective of sample density. This value concurs with that typically used for silica sands. As also shown in Fig. 10, in spite of their lower densities in some cases, MICP-treated samples with D_{rc} = 7–38% registered higher V_S than the untreated samples. For the treated sand, the ultimate V_S increases from a minimum of 246 m/s to a maximum of 395 m/s with increasing σ'_{vc} from 100 to 900 kPa. This corresponds to β = 0.19 fitted to V_S measured in the MICP-treated samples. Fig. 10 further shows increases

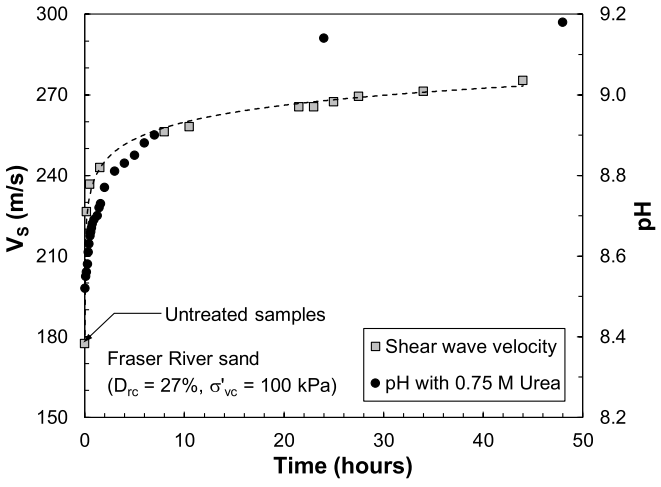

Fig. 9. Increases of V_S and pH immediately after the application of MICP treatment and a subsequent 48-h period for a Fraser River sand sample.

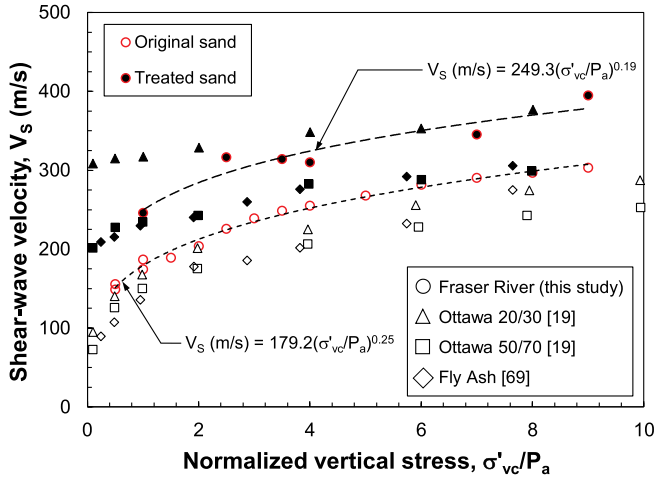

Fig. 10. Increases of V_S with normalized σ'_{vc} showing the effect of MICP treatment on Fraser River sand (this study), Ottawa 20/30 and Ottawa 50/70 sands [19], and fly ash [69].

in V_S with σ'_{vc} for microbially-treated samples of Ottawa 20/30 and Ottawa 50/70 sands [19] and fly ash [69], which are more or less comparable to those measured in this study for Fraser River sand.

4.2. SEM images

SEM images were taken to corroborate the DSS test results by examining the microstructural fabric and the pattern of calcium carbonate precipitation. Untreated and treated specimens were preserved and dried at 40 °C in an oven and then a cluster of particles were mounted on the SEM apparatus for imaging. Fig. 11 shows several SEM images of the treated samples. Particle-to-particle bonds are clearly visible in Fig. 11a and b, conforming with the observed increase of V_S in Fig. 9. Calcite crystals are also seen to have formed on particle surfaces as shown in the higher magnification images of Fig. 11c and d. Superior mechanical characteristics (e.g., strength, stiffness) are achieved when calcite is deposited at particle contacts, forming load-bearing bridges rather than at the location of individual bacterial cells [71–73]. In addition to particle cementation, these images show that precipitated calcite grains also occupy void spaces within the soil matrix, effectively densifying the sand matrix.

4.3. Cyclic DSS tests

The undrained cyclic shearing behaviour of the original untreated Fraser River sand is compared with that of the MICP-treated specimens consolidated to σ'_{vc} = 100 kPa. All medium-dense and dense samples (D_{rc} = 52% and 65%) were subjected to a repeated cyclic shearing stage to study post-liquefaction volumetric strains and the effect of a prior cyclic loading history on the re-liquefaction resistance of the treated sand.

Figs. 12 and 13 show typical cyclic stress paths and stress-strain responses of an untreated and a treated Fraser River sand samples subjected to the same σ'_{vc} = 100 kPa and CSR = 0.10. While the untreated sample undergoes large decrements of σ'_v particularly in the first stress cycle in Fig. 12, the MICP-treated sample demonstrates a much slower and a rather steady σ'_v reduction with each stress cycle in Fig. 13 which resembles a cyclic mobility type of behavior. The liquefaction failure criterion is defined here as the number of cycles (N_L) required to reach a single-amplitude shear strain (γ_{SA}) of 3.75% [65,67,74,75]. This strain level is equivalent to reaching a single-amplitude axial strain of 2.5% in a triaxial test, which is the definition of liquefaction adopted by the National Research Council [76]. As further indicated by the stress-strain curves, a total of 14 loading cycles were applied to reach liquefaction (at γ_{SA} = 3.75%) in the untreated specimen. Whereas, the treated specimen required a much larger N_L = 94 cycles to attain the liquefaction criterion

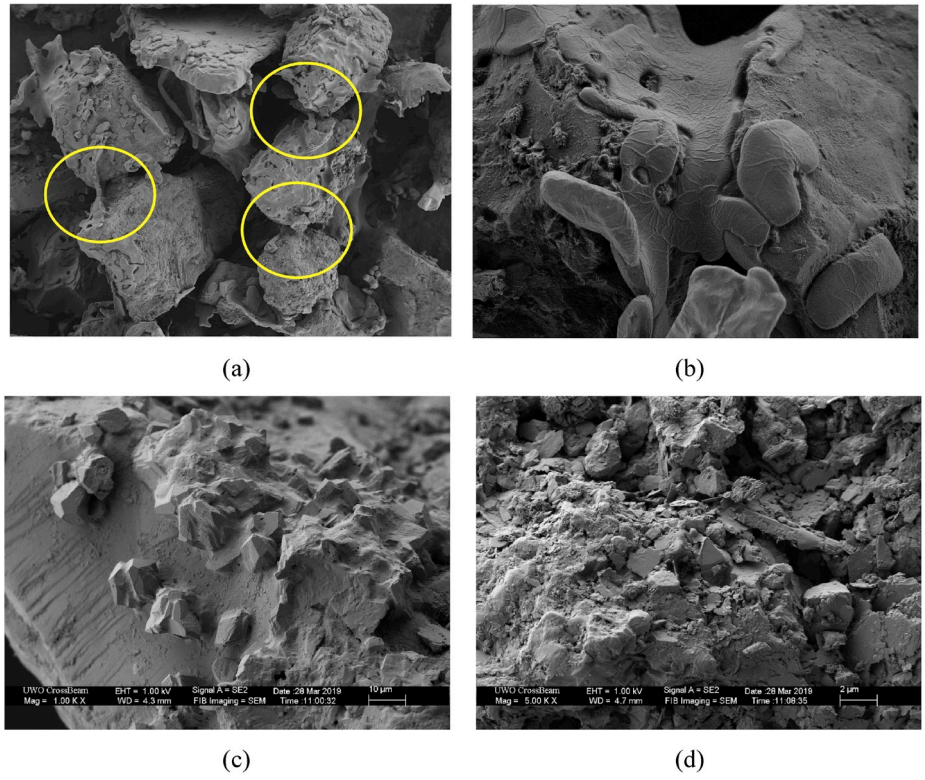

Fig. 11. SEM images of MICP-treated Fraser River sand highlighting (a and b) particle cementation at particle-to-particle contacts, and (c and d) increased particle angularity and surface roughness produced by $CaCO_3$ crystals on particle surfaces.

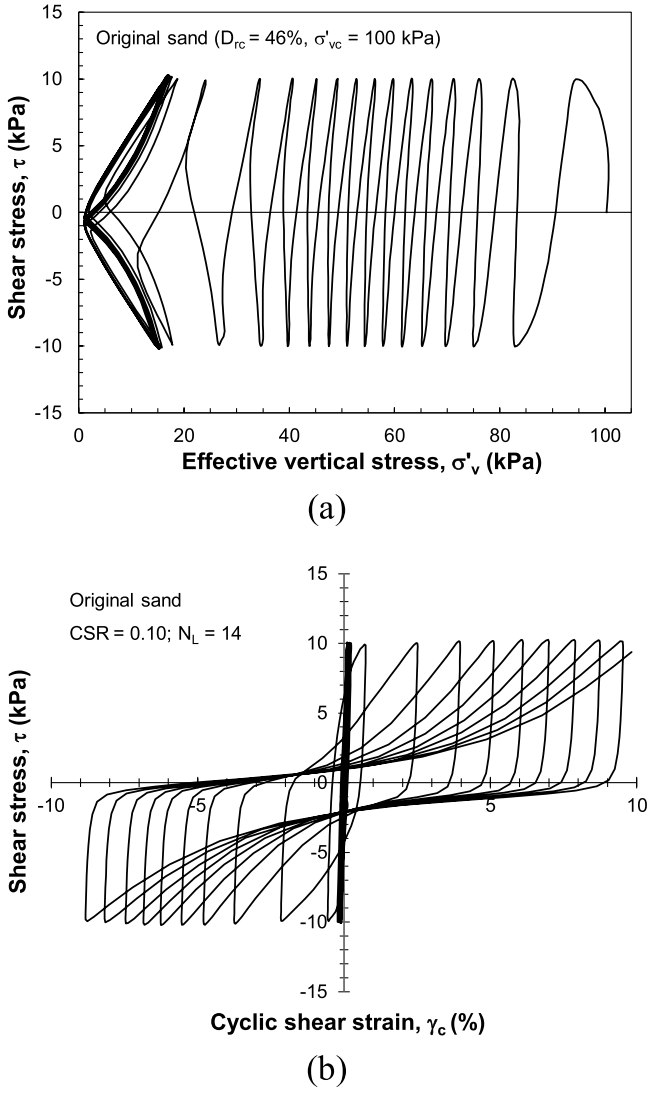

Fig. 12. Cyclic (a) stress path and (b) stress - strain response of an untreated Fraser River sand specimen consolidated to σ'_{vc} = 100 kPa and D_{rc} = 46% in a constant-volume DSS test subjected to CSR = 0.10.

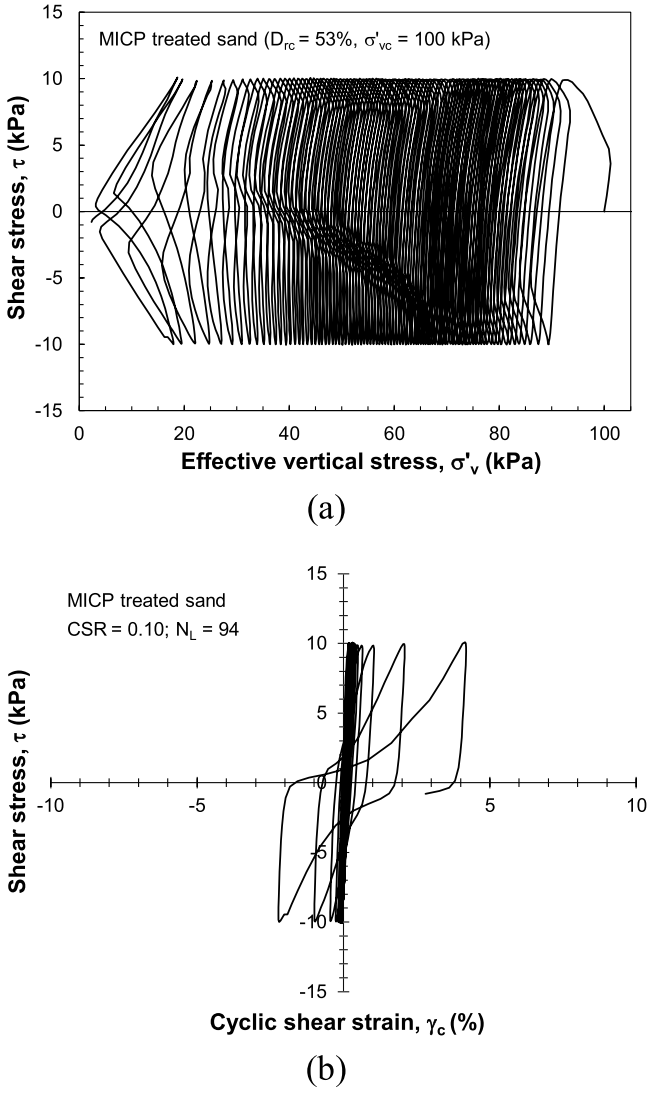

Fig. 13. Cyclic (a) stress path and (b) stress-strain response of an MICP-treated Fraser River sand specimen consolidated to σ'_{vc} = 100 kPa and D_{rc} = 53% in a constant-volume DSS test subjected to CSR = 0.10.

in Fig. 13, with most cycles confined to small strains (<0.5%). The shear strain progressively increased beyond $\gamma_{SA} \approx 0.5\%$ from the 92nd cycle until liquefaction was reached.

Given the importance of excess pore pressure generation on soil liquefaction due to cyclic loading [77–79], Fig. 14 shows the generation of equivalent pore pressure ratio, r_u (= $\Delta u/\sigma'_{vc}$) with N_L for treated and untreated specimens subjected to comparable CSR in the cyclic DSS tests. As demonstrated in this figure, the untreated sand samples display a sharp rise in r_u starting from the first few cycles, while those of the MICP-treated samples show a reduced rate of pore pressure generation, requiring a larger number of cycles to liquefaction. The rise of r_u in the treated samples resembles the characteristics of a dense sand, suggesting the higher dilatancy of these specimens due to particle cementation.

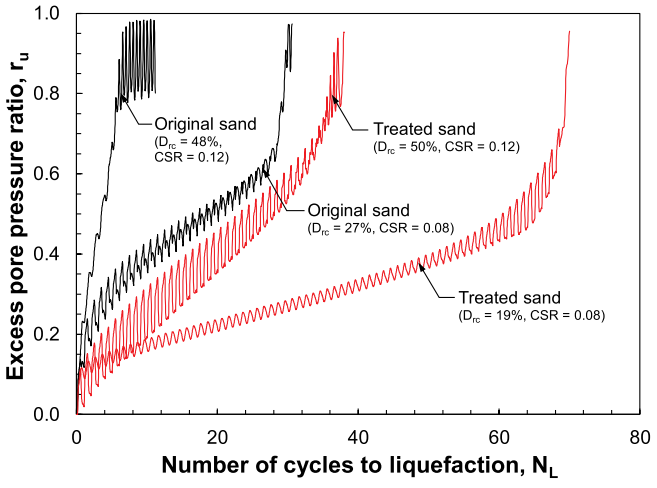

Fig. 14. Comparison of excess pore pressure ratios (r_u) versus the number of cycles to liquefaction (N_L) for untreated and MICP-treated specimens of Fraser River sand.

5. Discussion on the effects of MICP treatment

5.1. V_S and G_{max}

As previously described by Equation (2), V_S is primarily dependent on σ'_{vc}. The effect of σ'_{vc} on both untreated and treated samples was described in Fig. 10 by a power function, yielding β = 0.25 and 0.19,

respectively. Despite some scatter, Fig. 15 further shows a larger average $V_{S1} = 250$ m/s measured in the treated specimens compared to $V_{S1} \approx 179$ m/s of the original sand, without a strong trend with the consolidation void ratio (e_c). The observed increase in V_{S1} from 179 to 250 m/s would minimize liquefaction triggering potential in Fraser River sand [80,81].

The larger V_S values of MICP-treated samples are also indicative of their higher stiffness compared to the untreated sand. The maximum shear modulus (G_{max}) corresponding to small shear strains induced by a shear wave is estimated from V_S according to the following relationship:

$$G_{max}(MPa) = \rho V_S^2 \quad \text{(Eq. 3)}$$

where, ρ is the total density of the soil mass in kg/m^3. Fig. 16 compares G_{max} values of the untreated sand with those of the treated specimens. Same as V_S, treated samples show significantly larger G_{max} than those of the original sand as a result of particle cementation and stiffer particle contacts, with G_{max} consistently maintaining a gain of about 46 to 123 MPa. These are slightly lower than those measured by Nafisi and Montoya [82] in MICP-treated samples of Nevada sand ($D_{50} = 0.13$ mm; $D_{rc} = 40\%$) as illustrated in Fig. 16. This could be partly due to the one-dimensional consolidation of Fraser River sand samples in the DSS tests of this study as opposed to isotropic consolidation imposed on the Nevada sand samples in a triaxial cell.

The variations of G_{max} with σ'_{vc}/P_a for the samples of this study are further fitted with power functions in Fig. 16. While the stress exponent is about 0.50 for the untreated sand, it decreases to about 0.38 in the treated samples. This suggests a lower effect of σ'_{vc} on G_{max} (i.e., stiffness) measured in the MICP-treated samples as the sand particles are further restrained by the $CaCO_3$ cementation among them. Lower sensitivity of soil stiffness to effective stress is also reported by several other investigators for cemented sands [12,19,32,82,83]. For example, Chang and Woods [83] investigated the stress-dependency of G_{max} for an artificially-cemented sand and found that the stress exponent decreased with increasing the level of cementation. Lin et al. [19] examined the initial tangent Young's moduli obtained from the stress-strain curves of triaxial tests and found that the stress exponent reduced from 0.53 and 0.88 in respectively untreated Ottawa 20/30 and Ottawa 50/70 sands to 0.09 and 0.19 in MICP-treated samples of the same sands. In fact, the stress exponent of 0.38 obtained for the treated samples of Fraser River sand concurs with that suggested by Nafisi and Montoya [82] for lightly-cemented clean sands.

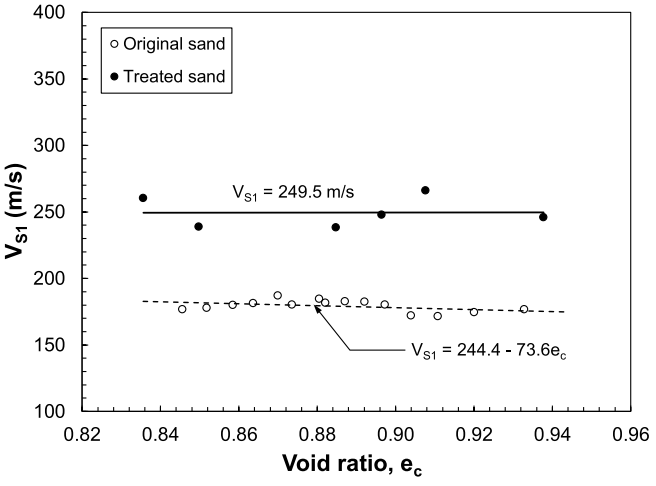

Fig. 15. Variations of V_{S1} with e_c in untreated and MICP-treated Fraser River sand samples.

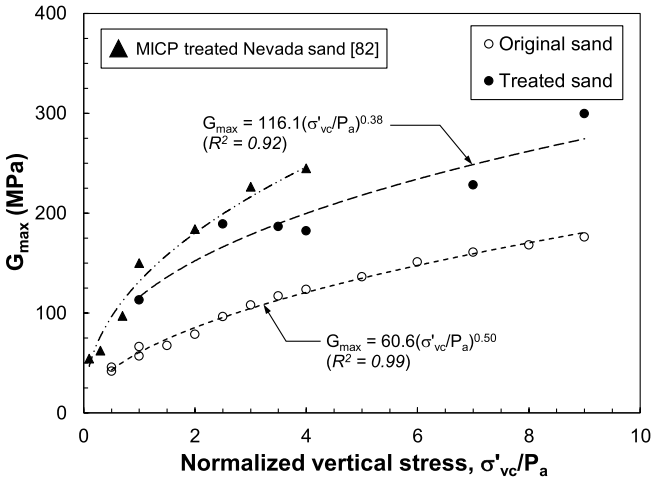

Fig. 16. Variations of G_{max} with normalized σ'_{vc} for the Fraser River sand of this study and Nevada sand [82] displaying the effect of MICP treatment.

5.2. Cyclic liquefaction behaviour

Figs. 17 to 19 compare the cyclic strength curves obtained for the original and the MICP-treated Fraser River sand specimens tested in this study. These figures show larger number of cycles (N_L) to reach the liquefaction criterion of $\gamma_{SA} = 3.75\%$ at a given CSR for the treated samples. This increased resistance results primarily from $CaCO_3$ cementation at particle-to-particle contacts, which helps to maintain most of the loading cycles at small shear strains (see Fig. 13) and reduces the rate of excess pore pressure generation (see Fig. 14) which eventually leads to liquefaction.

Because of densification during post-consolidation flushing of the specimens with the cementation reagent, precise control of D_{rc} was quite difficult in preparing the treated specimens. The resulting D_{rc} of the treated specimens are thus somewhat different than those of the original sand, particularly for the loose (Fig. 17) and the medium-dense (Fig. 18) tests. This may have produced some bias in examining the effect of MICP treatment on the cyclic strength curves of Figs. 17 to 19. To mitigate this bias, the cyclic stress ratio required to cause liquefaction in 15 cycles (CRR_{15}) is used here to compare the cyclic liquefaction resistances. This corresponds to an equivalent earthquake magnitude of 7.5 [84,85]. CRR_{15} is determined by fitting the cyclic strength curves with the following power function:

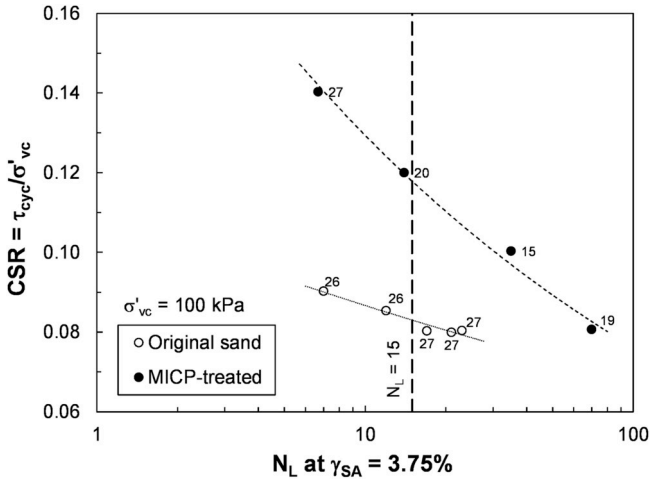

Fig. 17. Comparison of cyclic strength curves from DSS tests on untreated (D_{rc} = 26–27%) and MICP-treated (D_{rc} = 15–20%) samples of Fraser River sand. The number beside each datapoint shows D_{rc}.

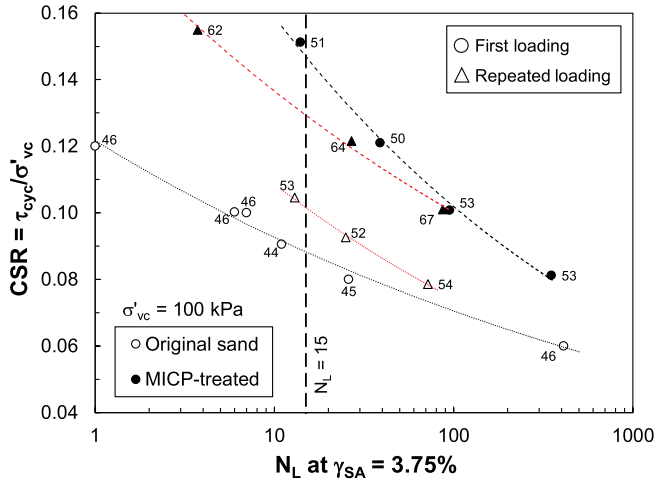

Fig. 18. Comparison of cyclic strength curves from DSS tests on untreated (D_{rc} = 44–46%) and MICP-treated (D_{rc} = 50–53%) samples of Fraser River sand. The number beside each datapoint shows D_{rc}.

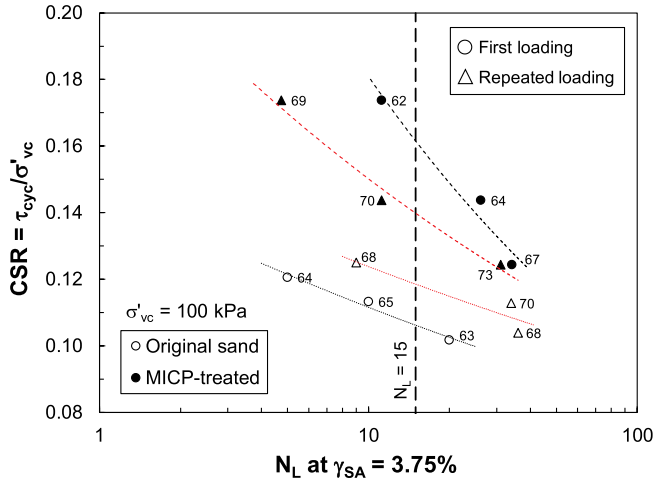

Fig. 19. Comparison of cyclic strength curves from DSS tests on untreated (D_{rc} = 63–65%) and MICP-treated (D_{rc} = 62–67%) samples of Fraser River sand. The number beside each datapoint shows D_{rc}.

$$CSR = a(N_L)^{-b} \quad \text{(Eq. 4)}$$

In which, coefficient "a" corresponds to the CSR which would produce liquefaction in one loading cycle (i.e., $N_L = 1$) and the exponent "b" describes the effect of soil characteristics on CSR. These fitting parameters are subsequently summarized in Table 2 for loose ($D_{rc} \leq 35\%$), medium-dense ($35 < D_{rc} \leq 60\%$) and dense ($60 < D_{rc} \leq 85\%$) sand samples. In addition to the higher ("a") coefficients shifting the cyclic strength curves of the treated samples to larger N_L, the relatively larger ("b") exponents reflect the steeper cyclic strength curves of the treated samples compared to those of the original sand. This suggests that the cyclic liquefaction resistance of the bio-cemented specimens has become more sensitive to N_L in comparison to the original untreated Fraser River sand.

Table 2
Summary of the parameters used to fit Equation (4) to data presented in Figs. 17 to 19

Sample density	Untreated		Treated	
	a	b	a	b
Loose	0.111	0.107	0.220	0.231
Medium-dense	0.122	0.118	0.248	0.193
Dense	0.148	0.122	0.345	0.281

Using the fitting parameters of Table 2 in Equation (4), Fig. 20 shows the variations of CRR_{15} with D_{rc}. Although the values of CRR_{15} for both the treated and the untreated sand increase with increasing D_{rc}, the trend established for the treated samples indicates a 42 to 67% improvement in CRR_{15} compared to that of the untreated sand. This improvement in liquefaction resistance stemming from a single treatment with MICP at a given D_{rc} is even greater than that achieved by only increasing D_{rc}.

5.3. Re-liquefaction resistance

The above discussion showed that MICP treatment can significantly reduce the liquefaction potential of Fraser River sand. Nevertheless, an in-situ sand deposit could experience a repeated cyclic loading in an aftershock or in a future seismic event. Whether the strengthening effect of MICP would remain following liquefaction, or diminish, requiring additional treatments could be a major concern. To address this question, untreated and MICP-treated specimens of medium-dense and dense Fraser River sand were subjected to a repeated cyclic loading. Following the first cyclic shearing in these tests, the shear stress was removed, the specimens were reconsolidated to $\sigma'_{vc} = 100$ kPa, and the same CSR was subsequently re-applied. For the untreated sand, Fig. 20 shows an increase in re-liquefaction resistance (i.e., requiring a higher N_L for a given CSR in Figs. 18 and 19) following post-liquefaction reconsolidation and densification of Fraser River sand samples. In contrast, a reduction occurs in the re-liquefaction resistance of the MICP-treated samples, requiring fewer N_L to liquefy despite a higher D_{rc} during the second cyclic loading application. This reduction probably occurs because of the breakage of the cementation bonds among sand particles. Nevertheless, the treated samples still show much higher resistances to cyclic loading than the untreated original sand. The SEM images previously shown in Fig. 11 indicate that $CaCO_3$ precipitation occurred on the surfaces of individual sand particles as a result of the treatment. Hence, not only were the particles bonded by $CaCO_3$ precipitated at particle-to-particle contacts, but also their surface roughness and angularity increased. Accordingly, the higher re-liquefaction resistance of the treated samples compared to that of the original Fraser River sand is perhaps the result of densification due to $CaCO_3$ precipitants, increased particle angularity and surface roughness, as well as some residual $CaCO_3$ particle-to-particle bonds. Therefore, the reinforcing effect of an MICP treatment may remain to a large extent – not principally through $CaCO_3$ bonds – and reduce the liquefaction potential of a treated sand

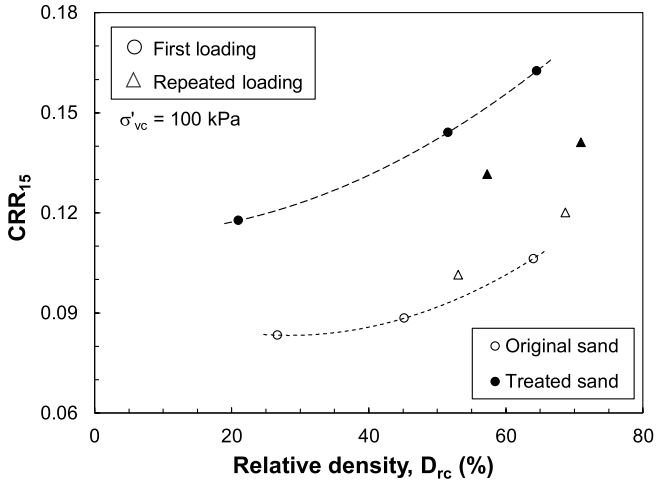

Fig. 20. Variations of CRR_{15} with D_{rc}.

deposit in a future seismic event. In general, the combined effects of cementation, increased particle angularity, and densification due to $CaCO_3$ precipitation produced a remarkable increase in Fraser River sand's resistance to cyclic loading.

5.4. Comparison with other studies

Differences in shearing mode, D_{rc}, effective stress level, and sand characteristics make a direct comparison between the CRR_{15} found here with those reported in other studies complicated. Changes in liquefaction resistance are thus compared through an improvement factor (I_F) defined as the ratio of CRR to produce liquefaction in a treated (CRR_t) sample over that of an untreated original (CRR_o) sand (i.e., $I_F = CRR_t/CRR_o$). These are plotted in Fig. 21 versus the number of cycles (N_L) to produce liquefaction. N_L can be related to the moment magnitude of an earthquake (M_w) with N_L = 22, 15, and 10 cycles corresponding to respectively M_w = 8.0, 7.5, and 7.0 [86]. For a given N_L, CRR is calculated from Equation (4) using the fitting parameters of Table 2.

The improvement factors found in this study are compared in Fig. 21 with those extracted from cyclic triaxial test results on MICP-treated samples of other clean sands [13,14,87], all consolidated to an isotropic confining stress of 100 kPa. The range of I_F (= 1.72 to 1.32) realized in Fraser River sand is generally comparable to or higher than those obtained for these other clean sands. However, the degrading trends of I_F with increasing N_L observed in the cyclic DSS tests of this study are opposite to the increasing values of I_F with N_L found from the cyclic triaxial tests. This difference could be due to a relatively higher resilience of the cementation bonds in simple shearing, requiring a larger CSR to break the bonds and induce liquefaction at lower number of cycles. Whereas, particle cementation bonds are readily crushed under compression loading, resulting in a relatively smaller gain in liquefaction resistance at lower N_L.

5.5. Post-liquefaction volumetric strain

An important feature of post-liquefaction behaviour is the accumulation of settlement as the shear-induced excess pore pressure dissipates. Liquefaction-induced ground settlement has often caused significant damages to critical lifelines and structures supported on shallow foundations in the past earthquakes. Post-earthquake settlement can be particularly detrimental if it occurs unevenly, resulting in differential settlement of buildings, foundations, bridge abutments, and underground structures. Settlements in the order of 10 to 20 cm have been documented in many sand deposits following previous earthquakes [88–91]. A classic example of liquefaction-induced settlement is the large tilting and settlement of more than 300 apartment buildings following the 1964 Niigata earthquake in Japan [92]. Differential settlement from the compression of loose sand pockets caused severe damage to major structures following the 1963 Skopke earthquake in Macedonia [91]. Large settlements also occurred following soil liquefaction in the 1960 Chilean earthquake [88] and the 1959 Jaltipan earthquake in Mexico [93]. Extensive settlement of buildings was observed in response to subsoil liquefaction following the 1990 Luzon earthquake at the city of Dagupan, Philippines [94,95]. Widespread ground settlement and lateral spreading also induced significant damage to buildings and underground utilities in the Marina District and Treasure Island of San Francisco following the 1989 Loma Prieta earthquake [96]. Subsoil liquefaction also caused many buildings in the Adapazari City of Northwestern Turkey to settle or tilt in the aftermath of the Kocaeli earthquake of August 17, 1999.

Post-liquefaction reconsolidation vertical strains (ε'_v) were measured in the medium-dense and dense specimens by unloading the shear stress, and then reconsolidating the specimens to the original σ'_{vc} = 100 kPa. Because of the lateral constraint imposed by the stack of annular rings around the sample, ε'_v is essentially equal to the reconsolidation volumetric strain (ε'_{vol}). This would represent ε'_{vol} for a nearly level-ground sand deposit (far away from any free face with little or no lateral displacement), beneath a wide building, or in a deep sublayer. Fig. 22 shows the variations of ε'_{vol} with the maximum shear strain (γ_{max}) attained in the first cyclic loading stage on Fraser River sand samples subjected to different CSR. γ_{max} can be regarded as a measure of the amount of disturbance sustained by a soil deposit following an earthquake. According to this figure, MICP treatment had little effect on ε'_{vol} probably because of the breakage of the interparticle cementations. This suggests that the residual $CaCO_3$ bonds and changes in particle texture and shape were inadequate to realize a positive reduction in the post-liquefaction compressibility and ε'_{vol} of the Fraser River sand specimens tested in this study. Irrespective of D_{rc}, CSR, or MICP treatment, Fig. 22 indicates the following range of relationships between ε'_{vol} and γ_{max}:

$$\varepsilon'_{vol} = (0.19 - 0.26)\gamma_{max} \quad \text{(Eq. 5)}$$

Although these data were obtained from uniformly loaded specimens, the type of cyclic loading (whether uniform or irregular), loading

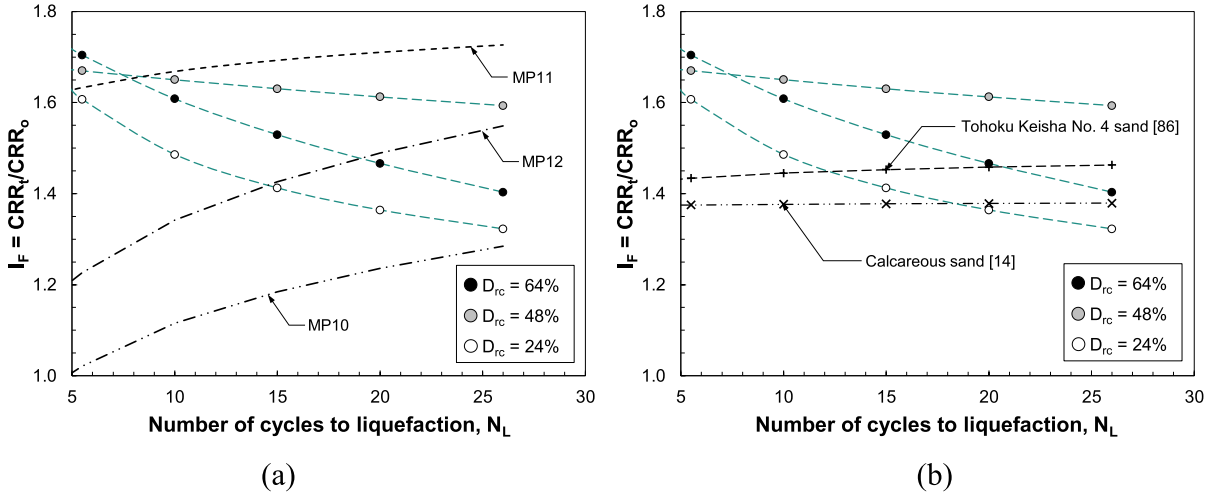

Fig. 21. Comparisons of improvement factors (I_F) found in the cyclic DSS tests of this study (green lines) with those extracted from cyclic triaxial tests on: (a) clean silica sand (D_{50} = 0.21 mm) specimens consolidated to D_{rc} = 30% and treated with different amounts of bacterial cell counts (MP10, MP11, MP12) by Han et al. [13], and (b) Tohoku Keisha No. 4 (D_{50} = 0.79 mm) sand [87] and a calcareous (D_{50} = 0.36 mm) sand from south China [14]. (For interpretation of the references to colour in this figure legend, the reader is referred to the web version of this article.)

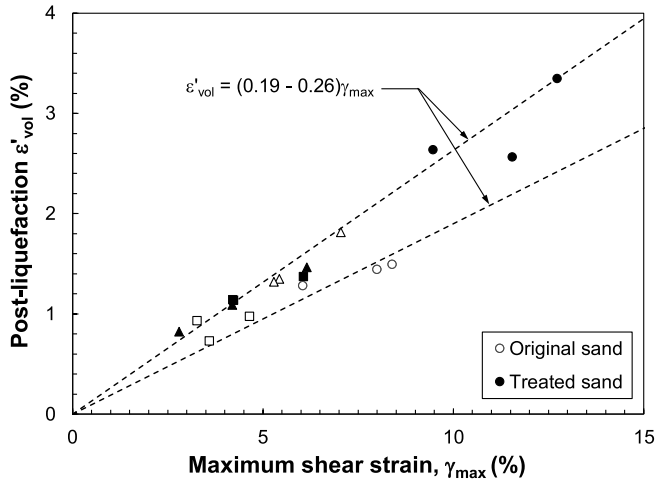

Fig. 22. Relationship between ε'_{vol} and γ_{max} measured in the cyclic DSS tests on Fraser River sand specimens.

frequency, and saturation are generally found to have negligible effects on the $\varepsilon'_{vol} - \gamma_{max}$ relationship for sands [97,98]. A strong effect of γ_{max} on ε'_{vol} has been also reported by several other investigators [97–106] in cyclic DSS tests. Furthermore, the range of ε'_{vol} (= 0.8–3.3%) shown in Fig. 22 for Fraser River sand is consistent with those reported by several other investigators in laboratory element tests [75,99,102,107], shaking table experiments [91,108], or from field observations [77,89,97,99,102,109]. For example, Nagase and Ishihara [102] measured ε'_{vol} = 4.0%, 2.5%, and 1.2% following cyclic DSS tests on specimens of Fuji River sand prepared at D_{rc} = 47%, 73%, and 93%, respectively. According to field measurements, re-consolidation of a 12.1 m deep sand fill resulted in level-ground surface settlements of 0.10 to 0.15 m following the 1971 San Francisco earthquake [91], which correspond to ε'_{vol} = 0.8–1.2%.

As discussed above, we have demonstrated the successful application of MICP for improving the liquefaction resistance and stiffness of Fraser River sand. This technique can be used as a more attractive and less expensive ground improvement method to mitigate soil liquefaction in the Fraser River delta and the lower mainland British Columbia. MICP is an environmental-friendly and sustainable natural process which uses a microorganism abundant in soil. Compared to most conventional ground improvement methods (e.g., stone columns, deep dynamic compaction, vibro-replacement, deep soil mixing, chemical grouting), MICP has little adverse environmental impacts (e.g., air or water pollution, excessive vibration, greenhouse gas emission) and can be applied both prior to and after construction beneath new or existing buildings and other infrastructure. The raw material (bacteria, urea, calcium source) for bio-cementation are also relatively cheap and economical [110]. These would allow a sustainable growth of the Fraser River delta while protecting existing natural resources and the environment.

6. Conclusions

In this study, a single application of a microbially-induced calcite precipitation (MICP) treatment was successfully employed to alter the behavior of Fraser River sand. X-Ray diffraction analysis of the precipitated $CaCO_3$ indicated that calcite and vaterite were the primary mineral phases produced by the treatment. Microscopic images of the treated samples showed clear evidences of cementation not only coating particle surfaces but also at particle contacts. Calcite crystal faces formed around the microorganisms were also visible in the highly magnified images. Principally as a result of the higher stiffness produced by particle cementation, shear-wave velocities (V_S) of the sand at various effective stresses increased by about 31% with a single cycle of the treatment. The corresponding gain in maximum shear modulus (G_{max}) ranged from 46 to 123 MPa, with a lower sensitivity to changes in effective stress.

The MICP treatment improved the sand's resistance against pore water pressure generation and cyclic liquefaction, as indicated by the larger number of cycles required to induce liquefaction. The pattern of excess pore pressure generation with the number of cycles showed a dramatic change from a sharp rise in r_u to a more gradual and steady increase with number of cycles. This suggests a change of the failure mechanism from liquefaction failure in the untreated sand to cyclic mobility in the MICP-treated samples. The results suggest that microbial cementation can be more effective for mitigating the risk of liquefaction in Fraser River sand than soil densification alone.

Furthermore, re-liquefaction of treated medium-dense and dense specimens showed a small decrease in cyclic resistance from that exhibited in the first liquefaction event, perhaps due to breakage of the $CaCO_3$ bonds following the first cyclic loading. Nonetheless, the strengthening effect of MICP treatment was shown to mostly remain, plausibly because of residual unbroken bonds and densification, thus continuing to reduce the liquefaction potential of a treated sand deposit in a future seismic event. Lastly, post-liquefaction settlement, measured as the volumetric strain produced after the first cyclic loading, was shown to be unaffected by the treatment, as it was seen to follow the same direct relationship with the maximum shear strain as the original sand.

With the promising application to Fraser River sand, MICP can be implemented as a sustainable and a more economical approach to improve the engineering properties of a Fraser River sand deposit for liquefaction mitigation.

Funding

This work was supported by the Ontario Ministry of Research and Innovation, Early Researchers Award, Round 11.

Declaration of competing interest

The authors declare that they have no known competing financial interests or personal relationships that could have appeared to influence the work reported in this paper.

CRediT authorship contribution statement

Guillermo Alexander Riveros: Methodology, Validation, Formal analysis, Investigation, Data curation, Writing - original draft, Visualization. **Abouzar Sadrekarimi:** Conceptualization, Investigation, Resources, Writing - review & editing, Visualization, Supervision, Project administration, Funding acquisition.

Appendix A. Supplementary data

Supplementary data to this article can be found online at https://doi.org/10.1016/j.soildyn.2020.106034.

References

[1] Weast RC, Astle MJ. CRC handbook of chemistry and physics : a ready-reference book of chemical and physical data. 63rd Edition ed. Boca Raton, Florida: CRC Press; 1982.
[2] Bosak T, Stolarski J, Meiborn A. Microbial formation and degradation of carbonates. In: Ehrlich HL, Newman DK, Kappler A, editors. Ehrlich's geomicrobiology. Chapman and Hall/CRC; 2015. p. 209–36.
[3] Chafetz HS, Buczynski C. Bacterially induced lithification of microbial mats. Arch Mikrobiol 1992;7:277–93.
[4] Krumbein WE. On the precipitation of aragonite on the surface of marine bacteria. Naturwissenschaften 1974;61. 167 - 167.

[5] Monty CL. Recent algal stromatolitic deposits, Andros Island, Bahamas. Preliminary report. Geol Rundsch 1972;61:742–83.
[6] Stocks-Fischer S, Galinat JK, Bang SS. Microbiological precipitation of $CaCO_3$. Soil Biol Biochem 1999;31:1563–71.
[7] Anbu P, Kang CH, Shin YJ, So JS. Formations of calcium carbonate minerals by bacteria and its multiple applications. SpringerPlus 2016;5:1–26.
[8] Spanos N, Koutsoukos PG. The transformation of vaterite to calcite: effect of the conditions of the solution in contact with the mineral phase. Crystal Growth 1998;191:783–90.
[9] Ferris FG, Phoenix V, Fujita Y, Smith RW. Kinetics of calcite precipitation induced by ureolytic bacteria at 10 to 20°C in artificial groundwater. Geochim Cosmochim Ac Geochim Cosmochim Ac 2003;67:1701–22.
[10] Kantzas A, Stehmeier L, Marentette DF, Ferris FG, Jha KN, Mourtis FM. A novel method of sand consolidation through bacteriogenic mineral plugging. In: CIM annual technical conference, calgary; 1992.
[11] Burbank M, Weaver T, Lewis R, Williams T, Williams B, Crawford R. Geotechnical tests of sands following bioinduced calcite precipitation catalyzed by indigenous bacteria Journal of Geotechincal and Geoenvironmental Engineering. ASCE 2013; 139:928–36.
[12] Montoya BM, de Jong DJ, Boulanger RW. Dynamic response of liquefiable sand improved by microbial-induced calcite precipitation. Geotechnique 2013;63: 302–12.
[13] Han Z, Cheng X, Ma Q. An experimental study on dynamic response for MICP strengthening liquefiable sands. Earthq Eng Eng Vib 2016;15:673–9.
[14] Xiao P, Liu H, Xiao Y, Stuedlein AW, Evans TM. Liquefaction resistance of bio-cemented calcareous sand. Soil Dyn Earthq Eng 2018;107:9–19.
[15] Zamani A, Feng K, Montoya BM. Improved liquefaction resistance from microbial induced carbonate cementation. In: Geotechnical earthquake engineering and soil dynamics V GSP 290. American Society of Civil Engineers (ASCE); 2018. p. 296–303.
[16] Whiffin VS, van Paassen LA, Harkes MP. Microbial carbonate precipitation as a soil improvement technique. Geomicrobiol J 2007;24:417–23.
[17] Mitchell JK, Santamarina JC. Biological considerations in geotechnical engineering. J Geotech Geoenviron Eng 2005;131:1222–33.
[18] DeJong JT, Mortensen BM, Martinez BC, Nelson DC. Bio-mediated soil improvement. Ecol Eng 2010;36:197–210.
[19] Lin H, Suleiman MT, Brown DG, Kavazanjian E. Mechanical behavior of sands treated by microbially induced carbonate precipitation. Journal of Geotechincal and Geoenvironmental Engineering, ASCE 2016:142.
[20] B.C. Byrne PM, Anderson DL, Earthquake design in Richmond. Version II. University of British Columbia, Department of Civil Engineering; 1987. p. 90.
[21] Watts BD, Seyers WC, Stewart RA. Liquefaction susceptibility of Greater Vancouver area soils. In: Geotechnique and natural hazards. Vancouver, British Columbia: BiTech Publishers; 1992. p. 145–57.
[22] Christian HA. Seismic liquefaction potential of the southwestern margin of the Fraser River delta. In: Clague JJ, Luternauer JL, Mosher DC, editors. Geology and natural hazards of the Fraser River delta, British Columbia. Geological Survey of Canada; 1998. p. 231–40.
[23] Whitman W, Goodfellow M, Kämpfer P, Busse H-J, Trujillo M, Ludwig W, Suzuki K-i, Parte A. Bergey's manual of systematic bacteriology, ume 5. New York: Springer-Verlag; 2012. The Actinobacteria.
[24] Talaro KP. Foundations in microbiology. sixth ed. ed. Boston, MA: McGraw-Hill Higher Education; 2008.
[25] McCoy D, Cetin A, Hausinger R. Characterization of urease from Sporosarcina ureae. Arch Microbiol 1992;157:411–6.
[26] Goldman M, Wilson D. Growth of Sporosarcina ureae in defined media. FEMS (Fed Eur Microbiol Soc) Microbiol Lett 1977;2:113–5.
[27] Lee M, Soon NW, Khun TC, Ling HS. Bio-mediated soil improvement under various concentrationsof cementation reagents. Appl Mech Mater 2012;204–208: 326–9.
[28] Martinez BC, De Jong JT, Ginn TR, Montoya BM, Barkouki TH, Hunt C, Tanyu B, Major D. Experimental optimization of microbial-induced carbonate precipitation for soil improvement. J Geotechnical Geoenvironment Eng ASCE 2013;139: 587–98.
[29] Buikema ND. Stabilization of iron mine tailings through microbially induced calcite precipitation. In: Department of civil and environmental engineering, Michigan technological university; 2015.
[30] Sharmaa A, Ramkrishnan R. Study on effect of microbial induced calcite precipitates on strength of fine grained soils. Perspectives in Science 2016;8: 198–202.
[31] Gat D, Tsesarsky M, Shamir D, Ronen Z. Accelerated microbial-induced $CaCO_3$ precipitation in a defined coculture of ureolytic and non-ureolytic bacteria. Biogeosciences 2014;11:2561–9.
[32] Feng K, Montoya BM. Influence of confinement and cementation level on the behavior of microbial-induced calcite precipitated sands under monotonic drained loading. J Geotechnical Geoenvironment Eng ASCE 2016;142.
[33] Gorospe C, Han S, Kim S, Park J, Kang C, Jeong J, So J. Effects of different calcium salts on calcium carbonate crystal formation by Sporosarcina pasteurii KCTC 3558. Biotechnol Bioproc Eng 2013;18:903–8.
[34] De Yoreo JJ, Vekilov PG. Principles of crystal nucleation and growth. Rev Mineral Geochem 2003;54:57–93.
[35] Favre N, Christ ML, Pierre AC. Biocatalytic capture of CO_2 with carbonic anhydrase and its transformation to solid carbonate. J Mol Catal B Enzym 2009; 60:163–70.
[36] Mitchell JK, Soga K. Fundamentals of soil behavior. Wiley; 2013. p. 592.
[37] Gonzalez-Munoz MT, Rodriguez-Navarro C, Martinez-Ruiz F, Arias JM, Merroun ML, Rodriguez-Gallego M. Bacterial biomineralization: new insights from Myxococcus – induced mineral precipitation. Geol Soc Spec Publ 2010;336: 31–50.
[38] Rodriguez-Navarro C, Jimenez-Lopez C, Rodriguez-Navarro A, Gonzalez-Munoz MT, Rodriguez-Gallego M. Bacterially mediated mineralization of vaterite. Geochim Cosmochim Ac Geochim Cosmochim Ac 2007;71:1197–213.
[39] Turnbull AG. A thermochemical study of vaterite. Geochim Cosmochim Ac Geochim Cosmochim Ac 1973;37:1593–601.
[40] Brunson RJ, Chaback JJ. Vaterite formation during coal liquefaction. Chem Geol 1979;25:333–8.
[41] Sondi I, Salopek-Sondi B. Influence of the primary structure of enzymes on the formation of $CaCO_3$ polymorphs: a comparison of plant (Canavalia ensiformis) and bacterial (Bacilluspasteurii) ureases. Langmuir 2005;21:8876–82.
[42] Sitepu H, O'Connor BH, Li DJ. Comparative evaluation of the March and generalized spherical harmonic preferred orientation models using X-ray diffraction data for molybdite and calcite powders. J Appl Crystallogr 2005;38: 158–67.
[43] Kamhi SR. On the structure of vaterite $CaCO_3$. Acta Crystallogr 1963;16:770–2.
[44] Jones S, Sadrekarimi A, Kokan M. Verification and normalization of miniature cone penetration test results for Fraser River sand. In: GeoOttawa, 70th Canadian geotechnical conference, Ottawa; 2017.
[45] ASTM. Standard D422: standard test method for particle-size analysis of soils. In: Annual book of ASTM standards. West Conshohocken, PA: ASTM International; 2007.
[46] ASTM. Standard D854: standard test methods for specific gravity of soil solids by water pycnometer. In: Annual book of ASTM standards. West Conshohocken, PA: ASTM International; 2006.
[47] ASTM. Standard D4253: standard test methods for maximum index density and unit weight of soils using a vibratory table. In: Annual book of ASTM standards. West Conshohocken, PA: ASTM International; 2006.
[48] ASTM. Standard D4254: standard test methods for minimum index density and unit weight of soils and calculation of relative density. In: Annual book of ASTM standards. West Conshohocken, PA: ASTM International; 2006.
[49] Ibrahim AA, Kagawa T. Microscopic measurement of sand fabric from cyclic tests causing liquefaction. Geotech Test J 1991;14.
[50] Sasitharan S. Collapse behavior of very loose sand. Edmonton, Alberta: Department of Civil Engineering, University of Alberta; 1994.
[51] Pitman TD, Robertson PK, Sego DC. Influence of fines on the collapse of loose sands. Can Geotech J 1994;31:728–39.
[52] Okwadha GD, Li J. Optimum conditions for microbial carbonate precipitation. Chemosphere Chemosphere 2010;81:1143–8.
[53] Montoya BM, DeJong J. Stress-strain behavior of sands cemented by microbially induced calcite precipitation. J Geotechnical Geoenvironment Eng ASCE 2015; 141:1–10.
[54] Feng K, Montoya BM. Quantifying level of microbial-induced Cementation for cyclically loaded sand. J Geotechnical Geoenvironment Eng ASCE 2017:143.
[55] Viggiani G, Atkinson JH. Interpretation of bender element tests. Geotechnique 1995;45:149–54.
[56] Jovicic V, Coop MR. The measurement of stiffness anisotropy in clays with bender element tests in the triaxial apparatus. Geotechnical Testing Journal, ASTM 1998; 21:3–10.
[57] Brignoli EGM, Gotti M, Stokoe II KH. Measurement of shear waves in laboratory specimens by means of piezoelectric transducers. Geotechnical Testing Journal, ASTM 1996;19:384–97.
[58] Camacho-Tauta J, Cascante G, Fonseca VD, Santos J. Time and frequency domain evaluation of bender element systems. Geotechnique 2015;65:548–62.
[59] Arroyo M, Wood DM, Greening PD. Source near-field effects and pulse tests in soils samples. Geotechnique 2003;53:337–45.
[60] Sanchez-Salinero I, Roesset JM, Stokoe II. Analytical studies of body wave propagation and attenuation. Texas, Austin: University of Texas, Geotechnical Engineering Center; 1986. p. 272.
[61] Lee J-S, Santamarina JC. Bender elements: performance and signal interpretation. J Geotechnical Geoenvironment Eng ASCE 2005;131:1063–70.
[62] Bjerrum L, Landva A. Direct simple shear tests on Norwegian quick clay. Geotechnique 1966;16:1–20.
[63] Finn WDL, Vaid YP. Liquefaction potential from drained constant volume cyclic simple shear tests. In: Sixth world conference on earthquake engineering, New Delhi; 1977. p. 2157–62.
[64] Dyvik R, Berre T, Lacasse S, Raadim B. Comparison of truly undrained and constant volume direct simple shear tests. Geotechnique 1987;37:3–10.
[65] Vaid YP, Sivathayalan S. Static and cyclic liquefaction potential of Fraser River delta sand in simple shear and triaxial tests. Can Geotech J 1996;33:281–9.
[66] ASTM. Standard D6528: standard test method for consolidated undrained direct simple shear testing of cohesive soils. In: Annual book of ASTM standards, ASTM international, west conshohocken, PA; 2007.
[67] Wijewickreme D, Sriskandakumar S, Byrne P. Cyclic loading response of loose air-pluviated Fraser River sand for validation of numerical models simulating centrifuge tests. Can Geotech J 2005;42:550–61.
[68] Rutherford CJ. Development of a multi-directional direct simple shear testing device for characterization of the cyclic shear response of marine clays. In: Department of civil and environmental engineering, Texas A&M university, college station; 2012.
[69] Safavizadeh S, Montoya BM, Gabr MA. Effect of microbial induced calcium carbonate precipitation on compressibility and hydraulic conductivity of fly ash. In: IFCEE GSP 296. American Society of Civil Engineers (ASCE); 2018. p. 69–79.

[70] Robertson PK, Sasitharan S, Cunning JC, Sego DC. Shear-wave velocity to evaluate in-situ state of Ottawa sand. J Geotechnical Eng ASCE 1995;121:262–73.
[71] DeJong JT, Martinez BM. Bio-mediated soil improvement: load transfer mechanisms at the micro- and macro-scales. Advances in ground improvement: Research to practice in the United States and China, vol. 188. ASCE GSP; 2009. p. 242–51.
[72] Al Qabany A, Soga K. Effect of chemical treatmentused in MICP on engineering properties of cemented soils. Geotechnique 2013;63:331–9.
[73] Cheng L, Cord-Ruwisch R, Shahin MA. Cementation of sand soil by microbially induced calcite precipitation at various degrees of saturation. Canadian Geotechincal Journal 2013;50:81–90.
[74] Lee KL, Seed HB. Cyclic stress conditions causing liquefaction of sand, soil mechanics and foundations division. ASCE 1967;93:47–70.
[75] Ishihara K. Liquefaction and flow failure during earthquakes. Geotechnique 1993; 43:351–415.
[76] National Research Council. Liquefaction of soils during earthquakes. Washington, D. C.: National Research Council Committee on Earthquake Engineering; 1985.
[77] Lee KL, Albaisa A. Earthquake induced settlements in saturated sands. J. Geotechnical Eng Div ASCE 1974;100:387–406.
[78] Seed BH, Martin PP, Lysmer J. The generation and dissipation of pore water pressures during soil liquefaction. In: Earthquake engineering Research center, berkeley, California; 1975. p. 46.
[79] Polito C, Green RA, Lee J. Pore pressure generation models for sands and silty soils subjected to cyclic loading. J Geotechnical Geoenvironment Eng ASCE 2008; 134:1490–500.
[80] Andrus RD, Stokoe KH. Liquefaction resistance of soils from shear-wave velocity. J Geotech Geoenviron Eng 2000;126:1015–25.
[81] Kayen R, Moss RES, Thompson EM, Seed RB, Cetin KO, Der Kiureghian AK, Tanaka Y, Tokimatsu K. Shear-wave velocity-based probabilistic and deterministic asessment of seismic soil liquefaction potential. J Geotechnical Geoenvironment Eng ASCE 2013;139:407–19.
[82] Nafisi A, Montoya BM. A new framework for identifying cementation level of MICP-treated sands. In: Lemnitzer A, Stuedlein AW, Suleiman MT, editors. IFCEE 2018: recent developments in geotechnical engineering practice (GSP 296). Orlando, Florida: American Society of Civil Engineers (ASCE); 2018. p. 37–47.
[83] Chang T, Woods RD. Effect of confining pressure on shear modulus of cemented sand. In: Cakmak AS, editor. Developments in geotechnical engineering. Elsevier Applied Science; 1987. p. 193–208.
[84] Seed HB, Idriss IM. Ground motions and soil liquefaction during earthquakes. In: EERI monograph, earthquake engineering Research institute (EERI), berkeley, California; 1982.
[85] Arango I. Magnitude scaling factors for soil liquefaction evaluations. J Geotechnical Eng ASCE 1996;122:929–36.
[86] Idriss IM, Boulanger RW. Soil liquefaction during earthquakes. San Francisco: Earthquake Engineering Research Institute; 2008.
[87] Simatupang M, Okamura M. Liquefaction resistance of sand improved with calcite precipitation at different degree of saturation. In: 3rd international conference on performance-based design in earthquake geotechnical engineering (PBD-III), vancouver, BC. Canada; 2017.
[88] Duke CM, Leeds DJ. Response of soils, foundations, and earth structures to the Chilean earthquakes of 1960. Bull Seismol Soc Am 1963;53:309–57.
[89] Grantz A, Plafker G, Kachadoorian R. Alaska's good friday earthquake march 27, 1964. In: Geological survey circular 491. Washington, D. C.: United States Geological Survey; 1964. p. 9–24.
[90] Waller RM. Effects of the earthquake of march 27, 1964, in the homer area, Alaska. In: U.S. Geological survey professional paper 542-D; 1966. p. 28.
[91] Seed HB, Silver ML. Settlement of dry sands during earthquakes. J Soil Mech Foundation Div ASCE 1972;98:318–97.
[92] Yoshimi YK, Tokimatsu K. Settlement of buildings on saturated sand during earthquakes. Soils Found Soils Found 1977;17:23–38.
[93] Marsal RJ. Behaviour of a sandy uniform soil during the Jaltipan earthquake, Mexico. In: 5th international conference on soil mechanics and foundation engineering, paris, France; 1961.
[94] Ishihara K, Acacio A, Towhata I. Liquefaction-induced ground damage in dagupan in the july 16, 1990 Luzon earthquake. Soils Found Soils Found 1993;33:133–54.
[95] Tokimatsu K, Kojimaa H, Kuwayama S, Abe A, Midorikawa S. Liquefaction-induced damage to buildings in 1990 Luzon earthquake. J Geotechnical Eng ASCE 1994;120:290–307.
[96] Egan JA, Wang ZL. Liquefaction-related ground deformation and effects on facilities at treasure Island, san Francisco, during the 17 october 1989 loma Prieta earthquake. In: 3rd Japan – U.S. Workshop on earthquake resistant design of lifeline facilities and countermeasures for soil liquefaction; 1991. p. 57–76.
[97] Youd TL. Compaction of sands by repeated shear straining. Journal of Soil Mechanics and Foundations Division, ASCE 1972;98:709–25.
[98] Tsukamoto Y, Ishihara K, Sawada S. Settlement of silty sand deposits following liquefaction during earthquakes. Soils Found Soils Found 2004;44:135–48.
[99] Silver ML, Seed HB. Volume changes in sands during cyclic loading. J Soil Mech Foundation Div ASCE 1971;97:1171–82.
[100] Martin GR, Finn WDL, Seed HB. Fundamentals of liquefaction under cyclic loading. J Geotech Eng Div 1975;101:423–38.
[101] Tatsuoka F, Sasaki T, Yamada S. Settlement in saturated sand induced by cyclic undrained simple shear. In: World conference on earthquake engineering; 1984. p. 95–102.
[102] Nagase H, Ishihara K. Liquefaction-induced compaction and settlementof sand during earthquakes. Soils Found Soils Found 1988;28:65–76.
[103] Vaid YP, Thomas J. Liquefaction and postliquefaction behavior of sand. J Geotechnical Eng ASCE 1995;121:163–73.
[104] Matsuda H, Shinozaki H, Okada N, Takamiya K, Shinyama K. Effects of multi-directional cyclic shear on the postearthquake settlement of ground. In: 13th world conference on earthquake engineering, vancouver, B.C., Canada; 2004. p. 2890.
[105] Sriskandakumar S. Cyclic loading response of Fraser River sand for validating of numerical models simulating centrifuge tests. In: Department of civil engineering, university of British Columbia, vancouver, BC; 2004.
[106] Ishihara K, Harada K, Lee WF, Chan CC, Safiullahe AMM. Post-liquefaction settlement analyses based on the volume change characteristics of undisturbed and reconstituted samples. Soils Found Soils Found 2016;56:533–46.
[107] Yoshimi Y. An experimental study of liquefaction of saturated sands. Soils Found Soils Found 1967;7:20–32.
[108] Whitman RV. Summary of results from shaking table tests at University of Chile using a medium sand. In: Research report R70-25, soils publication No. 258, Massachusetts institute of technology, cambridge, Massachusetts; 1970.
[109] Ohasaki Y. Effects of sand compaction on liquefaction during the Tokachioki earthquake. Soils Found Soils Found 1970;10:112–28.
[110] Ivanov V, Chu J. Applications of microorganisms to geotechnical engineering for bioclogging and biocementation of soil in-situ. Rev Environ Sci Biotechnol 2008; 7:139–53.